COMMUNICATIONS PHYSICS

ARTICLE

https://doi.org/10.1038/s42005-019-0194-9 OPEN

Excitons in InGaAs quantum dots without electron wetting layer states

Matthias C. Löbl[1], Sven Scholz[2], Immo Söllner[1], Julian Ritzmann[2], Thibaud Denneulin[3], András Kovács[3], Beata E. Kardynał[3], Andreas D. Wieck[2], Arne Ludwig[2] & Richard J. Warburton[1]

The Stranski–Krastanov growth-mode facilitates the self-assembly of quantum dots (QDs) by using lattice-mismatched semiconductors, for instance, InAs and GaAs. These QDs are excellent photon emitters: the optical decay of QD-excitons creates high-quality single-photons, which can be used for quantum communication. One significant drawback of the Stranski–Krastanov mode is the wetting layer. It results in a continuum close in energy to the confined states of the QD. The wetting-layer-states lead to scattering and dephasing of QD-excitons. Here, we report a slight modification to the Stranski–Krastanov growth-protocol of InAs on GaAs, which results in a radical change of the QD-properties. We demonstrate that the new QDs have no wetting-layer-continuum for electrons. They can host highly charged excitons where up to six electrons occupy the same QD. In addition, single QDs grown with this protocol exhibit optical linewidths matching those of the very best QDs making them an attractive alternative to conventional InGaAs QDs.

[1] Department of Physics, University of Basel, Klingelbergstrasse 82, CH-4056 Basel, Switzerland. [2] Lehrstuhl für Angewandte Festkörperphysik, Ruhr-Universität Bochum, DE-44780 Bochum, Germany. [3] Ernst Ruska-Centre for Microscopy and Spectroscopy, Peter Grünberg Institute, Forschungszentrum Jülich, DE-52425 Jülich, Germany. Correspondence and requests for materials should be addressed to M.C.L. (email: matthias.loebl@unibas.ch)

InGaAs quantum dots (QDs) grown in the Stranski–Krastanov (SK) mode are excellent photon emitters. Individual QDs provide a source of highly indistinguishable single-photons[1–6] and a platform for spin–photon and spin–spin entanglement[7–9]. Their solid-state nature enables the integration of QDs in on-chip nanostructures such as photonic crystal cavities or waveguides[10–15]. In some respects, a QD can be considered as an artificial atom. However, this approximation is often too simplistic. Unlike a real atom in free space, an exciton (a bound electron–hole pair) in a QD can couple to further degrees of freedom in its solid state environment, for instance, phonons[16–20] and nuclear spins[21–27]. One problematic source of unwanted coupling is the so-called wetting layer (WL)[28–31]. The WL is a two-dimensional layer lying between all QDs. It is an inherent feature of SK-growth.

On account of the confinement in the growth direction, there is an energy gap between the WL-continuum and QD-electron and QD-hole states. However, this gap protects the QD-electrons and -holes from coupling to the WL only to a certain extent. The gap vanishes for a QD containing several electrons due to the on-site Coulomb repulsion; the energy gap can be bridged by carrier–carrier and carrier–phonon scattering[28,32]. Furthermore, the gap is not complete: a low energy tail of the WL-continuum can extend to the QD-confined-states[33,34]. The result is that the WL has negative consequences for quantum applications: Multi-electron states of a QD hybridize with extended states of the WL[28,30,35], severely limiting the prospects for using multi-electron states as qubits, for instance, the four-electron qubit proposed in ref. [36]. A parasitic coupling between a QD and an off-resonant cavity[37,38] can be caused by QD–WL Auger processes[39,40]. The low-energy tail of WL-states[33,34] leads to damping of exciton Rabi oscillations[29,41,42] and enhanced exciton–phonon scattering[43]. Finally, the WL limits applications of small QDs where the QD-WL energy gap is small[44]. Such QDs are useful for a hybrid system of QDs and Cs-atoms[45,46].

We show here that the QD-properties can be radically altered when WL-states are absent. Electron WL-states are removed by a simple modification to the SK-growth: InGaAs QDs are overgrown with a monolayer of AlAs[47–50]. On the nanoscale, we propose that the absence of electron WL-states is related to the large bandgap of AlAs. Changes regarding the QD-properties are drastic: we observe highly charged excitons with narrow optical emission where up to six electrons occupy the conduction band shells of the QD—a novelty for QDs in the considered wavelength regime. The QD-potential is deepened and hybridization with any WL-continuum is absent. Furthermore, the QDs have close-to transform limited optical linewidths at low temperature, a very sensitive probe of the material quality[51]. Whenever the WL limits the QD-performance[29,37,40,41,43], we propose that conventional SK QDs can be profitably replaced with their no-electron WL-counterparts.

Results

Sample growth and ensemble measurements. The QDs are grown by molecular beam epitaxy on a GaAs-substrate with (001)-orientation. The first monolayer of InAs deposited on GaAs (at 525 °C) adopts the GaAs lattice constant. After deposition of 1.5 monolayers, the strain mismatch between InAs and GaAs leads to island formation[52] (Fig. 1a, b). These islands become optically-active QDs upon capping with GaAs. A two-dimensional InAs layer remains, the WL. This is the widely used SK self-assembly process.

Here, the InAs islands are capped initially with a single monolayer of AlAs which has a higher bandgap than GaAs (Fig. 1c). Subsequently, a capping layer of 2.0 nm GaAs is grown (at 500 °C) (Fig. 1d). The additional AlAs monolayer is the only change of the standard SK protocol. For some samples, a "flushing step"[53] is made following the growth of the GaAs-cap (increase of temperature to 630 °C) (Fig. 1e). With or without flushing, the heterostructure is completed with overgrowth of GaAs (Fig. 1f).

To determine the QD-structure post growth, we carried out scanning transmission electron microscopy (STEM). Figure 1g is a high-resolution high-angle annular dark-field STEM-image where the contrast is related to the atomic number. The QD is the ~3 nm high and ~30 nm wide bright feature close to the center of the image. The complete images with an atomic resolution demonstrate that the entire structure is defect-free (see Supplementary Note 1). The WL consists of InGaAs with a monolayer of AlAs contained within it. The AlAs capping layer can be clearly made out as a darker region surrounding the QD. Energy dispersive X-ray spectroscopy confirms the WL composition: indium atoms are found over a 2–3 nm thick region, yet the aluminum atoms are located within a 1 nm thick layer (Fig. 1h). These features point to highly mobile In atoms yet weakly mobile Al atoms under these growth conditions[54]. The overall thickness of the modified WL is similar to the WL of standard InGaAs QDs[55]. The In above the AlAs-layer is most likely due to In-segregation as illustrated in Fig. 1c–e. The STEM-image does not indicate a transition to a Volmer–Weber growth as found in ref. 48.

We probe the electronic states initially by photoluminescence (PL) experiments. Figure 1i shows ensemble PL from QDs grown with and without the AlAs-cap, in both cases without a flushing step. The spectra reveal the different shells (*s*, *p*, *d*) of the QDs. For the standard QDs, PL from the WL can be observed at ~925 nm, emission at lower wavelength is from bulk GaAs. In contrast, for the AlAs-capped QDs, the WL PL disappears. This is the first evidence for the absence of carrier confinement in the modified WL. We come to the same conclusion on flushed QDs for which the ensemble-PL is blue-shifted from 1000–1300 nm to ~900–980 nm (Fig. 1j). Without the AlAs-capping, there is strong emission from the WL at ~875 nm. For the AlAs-capped QDs, WL emission is not observed.

PL as a function of gate voltage. The ensemble-PL measurements do not distinguish between electron and hole confinement. We make this distinction by single-QD measurements. The particular concept is to probe the QD- and WL-electron-states by gradually lowering the energy of the states with respect to the Fermi energy of a tunnel-coupled[41,56–58] Fermi sea. The QD is small enough to exhibit pronounced Coulomb blockade: electrons from the Fermi sea are added one-by-one and the QD-states are filled according to Hund's rules[28,59]. A hole in the QD is provided by optical excitation with an above band laser (750 nm). We focus on flushed QDs, both without and with the AlAs capping layer.

For a standard InGaAs QD, PL as a function of gate voltage is shown in Fig. 2a. The plateaus correspond to different charge states of the QD-exciton (Fig. 2b): in the presence of a hole, electrons fill the QD-shells sequentially. The standard QD shows charging of the neutral exciton X^0 to a net charge of $-3e$, the exciton X^{3-} containing a total of four electrons and one hole. At higher gate voltage, the QD PL disappears. This is a sign that the WL becomes occupied[31,35,59–61].

The PL from the AlAs-capped QD is strikingly different. Charging beyond X^{3-} to X^{4-} and X^{5-} takes place (Fig. 2c, Supplementary Note 5). The X^{5-} contains a total of six electrons with fully occupied *s*- and *p*-shells. This is a novelty for QDs in this wavelength regime (960 nm). Further, even the X^{4-} and X^{5-} result in sharp emission lines and there is no rapid loss of intensity or rapid increase in linewidth at high gate voltages. This

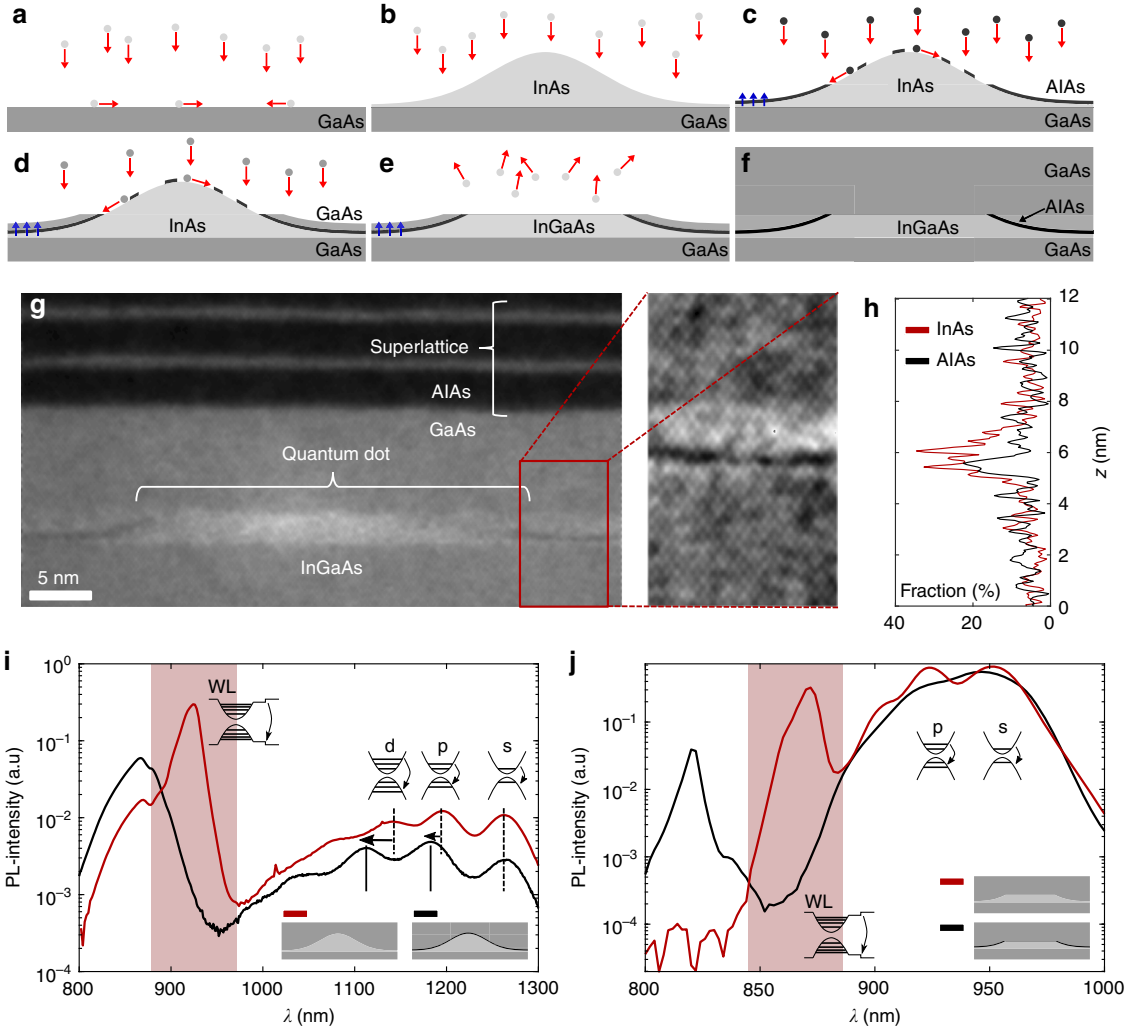

Fig. 1 Growth and characterization of the quantum dots. **a**–**f** Schematic process of the quantum dot (QD) growth. **a** InAs is deposited on a GaAs-surface. **b** After deposition of ~1.5 monolayers of InAs, strain-driven QD-formation takes place. The QDs are capped with a monolayer of AlAs (**c**) and 2 nm GaAs (**d**). During these steps segregation of In atoms takes place (blue arrows) resulting in a wetting layer (WL) which is an alloy of GaAs, InAs, and AlAs. **e** The top part of the capped QD evaporates at 630 °C (flushing step). **f** The flushed QDs are overgrown with GaAs. **g** Scanning transmission electron microscopy image of a flushed QD. InAs appears bright, AlAs dark. **h** Chemical composition of the WL measured by spatially resolved energy dispersive X-ray (EDX) spectroscopy at a location without a QD (different location to **g** but nominally the same). **i** Ensemble photoluminescence (PL) at room temperature from a sample with unflushed, standard InGaAs QDs (red curve) and unflushed, AlAs-capped InGaAs QDs (black curve). The WL PL (highlighted by the red band) dominates the spectrum. The QD PL appears in the regime 1000–1300 nm. The QD-shells are labeled. **j** Ensemble-PL at 77 K from a sample with flushed, standard InGaAs QDs (red curve) and flushed, AlAs-capped InGaAs QDs (black curve). The flushing blue-shifts the QD-ensemble to ~900–980 nm

measurement points to, first, a deep confinement potential, sufficiently deep to accommodate six electrons despite the strong Coulomb repulsions, and second, the absence of WL-states for electrons.

At high positive bias, PL appears also at ~830 nm (see Supplementary Fig. 2), highly blue-shifted with respect to the QD PL, and close to the bandgap of GaAs. This PL line has a very strong Stark shift allowing us to identify it as a spatially indirect transition[31,62] from an electron in the Fermi sea with a hole in the WL. From this line, we can, therefore, extract the properties of the WL in the valence band. We find that the AlAs-capped QDs have a valence band WL with ionization energy 19 meV with respect to the top of the GaAs valence band (see Supplementary Note 2). This ionization energy is reduced with respect to the WL of standard InGaAs QDs (ionization energy ~30 meV). The AlAs-cap eliminates any bound WL-states in the conduction band and pushes the bound WL-states in the valence band towards the GaAs valence band edge.

The full theoretical explanation for the absence of electron WL-states requires consideration of strain[63] and, possibly, a treatment beyond the envelope wavefunction approximation[64]. This is left for future investigations.

Triply-charged excitons. For standard InGaAs QDs (Fig. 3a) and AlAs-capped QDs (Fig. 3b), we measure PL of the X^{3-}-exciton as a function of the magnetic field parallel to the growth direction.

We present a method to probe the high-lying energy states, for instance, the QD-*d*-shell and WL-states, without occupying them. The method relies on an imbalance with respect to shell filling in the X^{3-} final state. Following X^{3-} recombination, there are two *p*-shell electrons yet just one *s*-shell electron. (Of the two *s*-shell electrons in the X^{3-} initial state, one recombines with the hole to create a photon.) This imbalance enables Auger-like processes: one of the *p*-shell electrons falls into the *s*-shell thereby losing energy; the other *p*-shell electron is given exactly this energy and

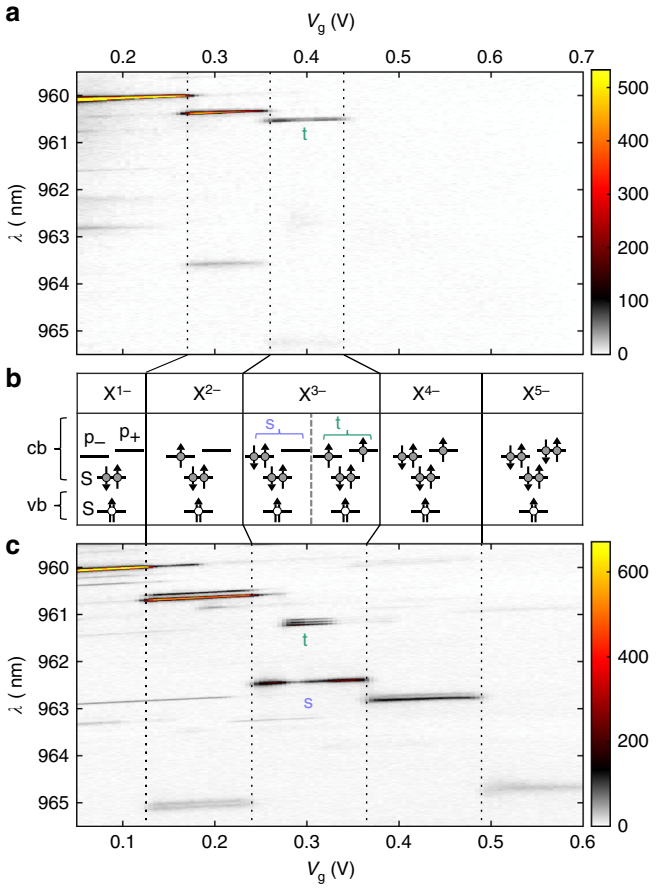

Fig. 2 Photoluminescence (PL) as electron states are sequentially filled. **a** PL counts versus gate voltage on a single, standard, flushed InGaAs quantum dot (QD). The plateaus correspond to Coulomb blockade[59]. **b** QD-shells and their occupation for the different exciton complexes. The triply charged exciton X^{3-} has two low-lying states: a singlet (blue: s) or a triplet (green: t). **c** PL counts versus gate voltage on a single, AlAs-capped, flushed InGaAs QD. In the absence of wetting layer states for electrons, the X^{3-} singlet (s) and triplet (t) as well as the highly charged exciton complexes X^{4-} and X^{5-} appear

is promoted to a higher-lying state (Fig. 3c). This process will only occur if a high-lying state exists close to the right energy. If the *s*–*p* separation is $\hbar\omega_0$, the process is, therefore, a probe of the energy levels lying $\hbar\omega_0$ above the *p*-shell. Some spectroscopy is possible: the energy levels of a QD can be tuned with a magnetic field. These processes can result in large changes to the PL on charging from X^{2-} to X^{3-}[28,30]. For instance, in a QD without a *d*-shell, on applying a magnetic field, the X^{3-} PL shows a series of pronounced anti-crossings with Landau levels associated with the WL[28]: the WL is thereby probed without occupying it.

We explore initially X^{3-} on standard InGaAs QDs. For the singly and doubly charged excitons, X^{1-} and X^{2-}, the emission splits into two lines by the Zeeman effect and blue-shifts via its diamagnetic response (see Supplementary Fig. 5). The X^{3-} has a much richer structure (Fig. 3a). At zero magnetic field, the X^{3-} has a configuration with two electrons in the QD-*s*-shell and two electrons in the *p*-shell. According to Hund's rules, the ground state electrons occupy different *p*-sub-shells with parallel spins (a spin-triplet) and two emission lines result, split by the large electron–electron exchange energy, denoted as *t* (triplet) and t_s (triplet satellite) in Fig. 3a[28]. On increasing the magnetic field, the degeneracy (or near degeneracy) of the *p*-sub-shells is lifted. In the Fock–Darwin model[28,65,66], the p_--sub-shell (angular momentum $L_z = +1$) moves down in energy by $-\frac{1}{2}\hbar\omega_c$ while the p_+-sub-shell (angular momentum $L_z = -1$) moves up in energy by $+\frac{1}{2}\hbar\omega_c$ (Fig. 3d). Here, $\hbar\omega_c$ is the electron cyclotron energy. Once this splitting becomes large enough, the X^{3-} ground state turns from a triplet to a singlet where two electrons of opposite spin populate the lower *p*-sub-shell (Fig. 3d)[28]. The transition from triplet to singlet ground state occurs at ~1.3 T (Fig. 3a). The singlet (and not the triplet) ground state represents the probe of the higher lying electronic states.

The magnetic field dependence of the X^{3-} singlet-PL-spectrum on a standard InGaAs QD shows several anti-crossings (Fig. 3a). We develop a model to describe the X^{3-} final state including Coulomb interactions within a harmonic confinement and couplings to a WL-continuum (see Supplementary Note 3). In addition to the energies of the transitions, the linewidths are a powerful diagnostic. The spectrally narrow PL-lines arise from intra-QD-processes; the spectrally broad PL-lines from QD–WL-continuum coupling as the continuum of WL-states facilitates rapid dephasing[28,43].

The singlet emission at ~1.3 T is spectrally broad, which signifies that the final state couples to the WL-continuum. There is an anti-crossing at ~3 T with a state with a linear magnetic field dispersion. This anti-crossing indicates a hybridization with the 0th WL-Landau-level (Fig. 3e). A second singlet emission line appears at higher energy, and there are two further anti-crossings at a high magnetic field (A_1 and A_2 in Fig. 3a). We exclude that these processes are caused by hybridization with the WL since the optical emission stays narrow in this regime. The first part of the explanation is an Auger-like process within the QD itself (Fig. 3e). The optical decay of the X^{3-} singlet leaves behind two electrons in the lower *p*-sub-shell and one electron in the *s*-shell (state $|a\rangle$). This final state can couple to state $|b\rangle$ via an Auger-like process where one *p*-electron fills the vacancy in the *s*-shell and the other goes up into the *d*-shell. This coherent coupling between the two basis states $|a\rangle$ and $|b\rangle$ leads to two eigenstates after optical decay and thus explains the second emission line at higher energy. The second part of the explanation involves the single particle states. With increasing magnetic field, the d_--sub-shell of the QD moves down in energy with a dispersion of $-\hbar\omega_c$ while the p_+-sub-shell moves up with $\frac{1}{2}\hbar\omega_c$. In the Fock–Darwin model, angular momentum is a good quantum number and d_- and p_+ therefore cross. Experimentally, this is not the case: there is a small anti-crossing. This is not surprising for a real QD where there is no exact rotational symmetry. To describe this, we introduce basis state $|c\rangle$ (with an electron in the p_+- rather than the d_--shell) and a small coupling between states $|b\rangle$ and $|c\rangle$ to describe the symmetry breaking. This leads to the two characteristic anti-crossings (A_1, A_2) of the singlet emission pair with a line with a dispersion of approximately $-\frac{3}{2}\hbar\omega_c$.

An analytic Hamiltonian describing all these processes is given in Supplementary Note 3. Using realistic parameters for the QD, the model (Fig. 3a) reproduces the X^{3-} PL extremely well. This strong agreement allows us to extract the key QD parameters from this experiment: the electron *s*–*p* splitting ($\hbar\omega_0 = 24.1$ meV) and the electron effective mass ($0.07m_o$). We are also to conclude that the potential is subharmonic: the *p*–*d* splitting is smaller than the *s*–*p* splitting.

With this understanding of the X^{3-}, we turn to the spectra from an AlAs-capped QD (Fig. 3b). As for the standard InGaAs QD, there is a transition from triplet to singlet X^{3-} ground state, albeit at higher magnetic fields. In complete contrast to the standard InGaAs QD, the hybridization with a Landau level is not observed. This is powerful evidence that the electron WL-states no longer exist.

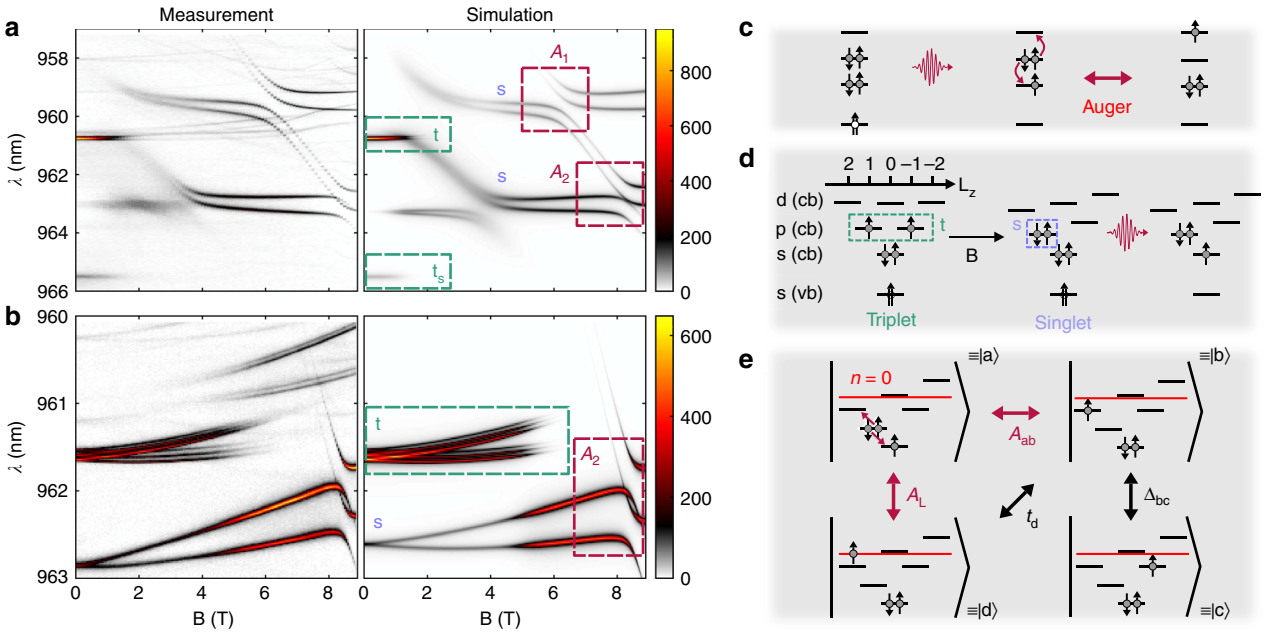

Fig. 3 Triply-charged exciton as a probe of the quantum dot (QD) and the wetting layer (WL) states. **a** X^{3-} counts as a function of the magnetic field for a standard InGaAs QD (measurement and simulation). **b** As (a) but for an AlAs-capped QD. Note that the line appearing at ~5 T and wavelength ~961 nm arises from X^{2-}, not X^{3-}. **c** The optical decay process of the X^{3-} singlet. Following photon emission, the *p*-shell is doubly occupied yet there is a vacancy in the *s*-shell. This turns on an Auger-like coupling to a state in which a high-lying level is singly occupied (QD-shell or WL-continuum) and the *s*-shell is doubly occupied. In this way, the PL-process is sensitive to the high-lying state even though it is not occupied in the initial state[28]. **d** X^{3-} assuming that angular momentum is a good quantum number: the *p*-shell has angular momentum $L_z = +1$ and -1; the *d*-shell $+2$, 0 and -2. The X^{3-} ground state changes from a triplet to a singlet at a finite magnetic field. **e** The final state of the singlet X^{3-}. State $|a\rangle$ can couple to the *d*-shell of the QD via an Auger-like process (state $|b\rangle$) and to a Landau level in the WL (state $|d\rangle$). When d_- and p_+ come into resonance, state $|b\rangle$ couples to state $|c\rangle$ where one electron occupies the p_+-sub-shell

The X^{3-} from the AlAs-capped QD is revealing in a number of other respects. First, the X^{3-} singlet state shows one Zeeman-split line, not two as for the standard InGaAs QD. This is evidence that the $|a\rangle$–$|b\rangle$ coupling is suppressed on account of the energies: state $|b\rangle$ lies at too high an energy to couple to state $|a\rangle$ (see Supplementary Note 3). A large ratio between $|b\rangle$–$|a\rangle$ energy splitting and coupling strength leads to a very weak emission from the second line, strongly red-shifted for a positive $|b\rangle$–$|a\rangle$ energy splitting. The absence of a second singlet emission line is evidence that the *p*–*d* splitting is larger than the *s*–*p* splitting, a superharmonic potential. This is consistent with the thin, AlAs-layer in the STEM-characterization (Fig. 1g) which bolsters the lateral confinement; and also the ensemble-PL where the AlAs-cap blue-shifts the *d*-shell more than the *p*-shell (Fig. 1i). Second, the X^{3-} singlet and triplet X^{3-}-PL-lines appear simultaneously at low magnetic field (Fig. 3b) yet there is a rather abrupt transition for the standard InGaAs QD (Fig. 3a). This is an indication that relaxation to the exciton ground state is slower for the AlAs-capped QDs. This may also be related to the WL: electrons in the WL can mediate spin relaxation and without the WL, this process is turned off. Finally, the X^{3-} exciton in the AlAs-capped QD has a very pronounced fine structure splitting: the splitting of the X^{3-} triplet into three lines is a prominent feature (Fig. 3b). This particular fine structure originates from the electron–hole exchange in the initial exciton state[60], and its increase relative to standard InGaAs QDs is indicative of a stronger electron–hole confinement[67,68].

We model X^{3-} in the AlAs-capped QD with the model developed for the standard InGaAs QD. The coupling to the Landau level is set to zero. A small perturbation is included to account for the anharmonicity of the confinement potential. The model describes the experimental results extremely well (Fig. 3b). The model determines the electron *s*–*p* splitting as $\hbar\omega_0 =$ 27.5 meV.

Temperature dependence. The temperature dependence of the exciton linewidths is a further probe of the coupling to continuum states. Linewidths of excitons in standard InGaAs QDs strongly increase with temperature as soon as hybridization with a WL is present[43]. Such a temperature broadening was observed for exciton complexes even with modest charge[43], for instance, X^{2-}. For an AlAs-capped QD, we measure the PL-linewidth of all charged excitons (X^{1-}–X^{5-}) as a function of temperature (Fig. 4a). Even for the highly charged excitons X^{4-} and X^{5-}, the temperature-induced broadening is much weaker than that for charged excitons beyond X^{1-} in standard InGaAs QDs which show a strong, linear temperature dependence[43]. Instead, the linewidths are described well by a model which considers a localized exciton and dephasing via acoustic phonon scattering[69]. This too is evidence that the WL-states for electrons no longer exist.

Finally, we measure the linewidth of the singly charged exciton (X^{1-}) with resonant excitation, detecting the resonance fluorescence[51] (Fig. 4b). The resonance fluorescence linewidth increases with temperature above ~10 K, indicative of acoustic phonon scattering (see Supplementary Note 4). At 4.2 K, the linewidth (2.3 μeV) is similar to the linewidth of the very best InGaAs QDs[51]. This shows that the AlAs-capped QDs retain the very low charge noise achieved for standard InGaAs QDs[51,70]. This is important: the AlAs-capped QDs have slow exciton dephasing and weak spectral fluctuations such that they are completely compatible with applications which place stringent requirements on the quality of the single-photons.

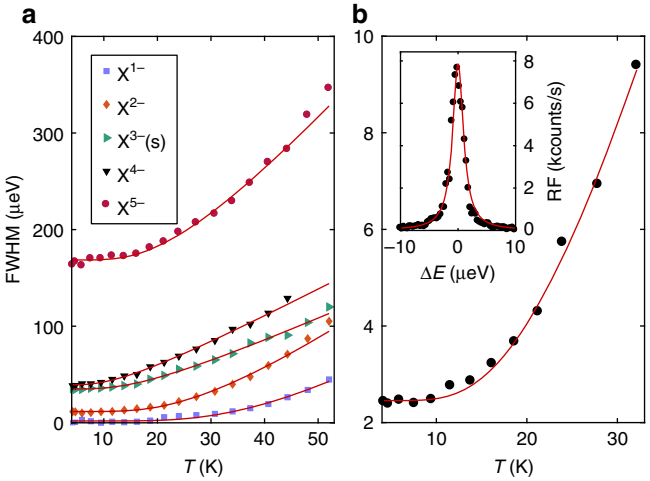

Fig. 4 Linewidths of excitons in an AlAs-capped quantum dot. **a** Photoluminescence-linewidth (full width at half maximum) of the charged excitons as a function of temperature. The red lines represent a fit to a model that describes the interaction with acoustic phonons. **b** Linewidth of the singly charged exciton X^{1-} in resonance fluorescence as a function of temperature. The inset shows an exemplary resonance fluorescence measurement at 4.2 K with a linewidth of 2.3 μeV. This measurement was carried out at low excitation power (coherent scattering regime). The saturation count rate obtained under resonant excitation is 60 kcounts/s

Data availability

The data that support the plots within this paper and other findings of this study are available from the corresponding author upon reasonable request.

Received: 20 June 2019 Accepted: 22 July 2019
Published online: 09 August 2019

References

1. Somaschi, N. et al. Near-optimal single-photon sources in the solid state. *Nat. Photonics* **10**, 340–345 (2016).
2. Ding, X. et al. On-demand single photons with high extraction efficiency and near-unity indistinguishability from a resonantly driven quantum dot in a micropillar. *Phys. Rev. Lett.* **116**, 020401 (2016).
3. Kiršanskė, G. et al. Indistinguishable and efficient single photons from a quantum dot in a planar nanobeam waveguide. *Phys. Rev. B* **96**, 165306 (2017).
4. Liu, F. et al. High purcell factor generation of indistinguishable on-chip single photons. *Nat. Nanotechnol.* **13**, 835 (2018).
5. He, Y.-M. et al. Deterministic implementation of a bright, on-demand single-photon source with near-unity indistinguishability via quantum dot imaging. *Optica* **4**, 802–808 (2017).
6. Müller, M., Bounouar, S., Jöns, K. D., Glässl, M. & Michler, P. On-demand generation of indistinguishable polarization-entangled photon pairs. *Nat. Photonics* **8**, 224 (2014).
7. Delteil, A. et al. Generation of heralded entanglement between distant hole spins. *Nat. Phys.* **12**, 218–223 (2016).
8. Gao, W. B., Fallahi, P., Togan, E., Miguel-Sanchez, J. & Imamoglu, A. Observation of entanglement between a quantum dot spin and a single photon. *Nature* **491**, 426–430 (2012).
9. Stockill, R. et al. Phase-tuned entangled state generation between distant spin qubits. *Phys. Rev. Lett.* **119**, 010503 (2017).
10. Lodahl, P., Mahmoodian, S. & Stobbe, S. Interfacing single photons and single quantum dots with photonic nanostructures. *Rev. Mod. Phys.* **87**, 347–400 (2015).
11. Englund, D. et al. Controlling the spontaneous emission rate of single quantum dots in a two-dimensional photonic crystal. *Phys. Rev. Lett.* **95**, 013904 (2005).
12. Volz, T. et al. Ultrafast all-optical switching by single photons. *Nat. Photonics* **6**, 605 (2012).
13. Arcari, M. et al. Near-unity coupling efficiency of a quantum emitter to a photonic crystal waveguide. *Phys. Rev. Lett.* **113**, 093603 (2014).
14. Vora, P. M. et al. Spin–cavity interactions between a quantum dot molecule and a photonic crystal cavity. *Nat. Commun.* **6**, 7665 (2015).
15. Javadi, A. et al. Spin–photon interface and spin-controlled photon switching in a nanobeam waveguide. *Nat. Nanotechnol.* **13**, 398 (2018).
16. Ramsay, A. J. et al. Phonon-induced Rabi-frequency renormalization of optically driven single InGaAs/GaAs quantum dots. *Phys. Rev. Lett.* **105**, 177402 (2010).
17. Wei, Y.-J. et al. Deterministic and robust generation of single photons from a single quantum dot with 99.5% indistinguishability using adiabatic rapid passage. *Nano Lett.* **14**, 6515–6519 (2014).
18. Kaldewey, T. et al. Demonstrating the decoupling regime of the electron–phonon interaction in a quantum dot using chirped optical excitation. *Phys. Rev. B* **95**, 241306 (2017).
19. Brash, A. J. et al. Light scattering from solid-state quantum emitters: beyond the atomic picture. *arXiv:1904.05284* (2019).
20. Koong, Z.-X. et al. Fundamental limits to coherent photon generation with solid-state atom-like transitions. *arXiv:1904.05103* (2019).
21. Greilich, A. et al. Nuclei-induced frequency focusing of electron spin coherence. *Science* **317**, 1896–1899 (2007).
22. Press, D. et al. Ultrafast optical spin echo in a single quantum dot. *Nat. Photonics* **4**, 367–370 (2008).
23. Prechtel, J. H. et al. Decoupling a hole spin qubit from the nuclear spins. *Nat. Mater.* **15**, 981–986 (2016).
24. Wüst, G. et al. Role of the electron spin in determining the coherence of the nuclear spins in a quantum dot. *Nat. Nanotechnol.* **11**, 885 (2016).
25. Éthier-Majcher, G. et al. Improving a solid-state qubit through an engineered mesoscopic environment. *Phys. Rev. Lett.* **119**, 130503 (2017).
26. Huthmacher, L. et al. Coherence of a dynamically decoupled quantum-dot hole spin. *Phys. Rev. B* **97**, 241413 (2018).
27. Gangloff, D. et al. Quantum interface of an electron and a nuclear ensemble. *Science* **364**, 62–66 (2019).
28. Karrai, K. et al. Hybridization of electronic states in quantum dots through photon emission. *Nature* **427**, 135–138 (2003).
29. Wang, Q. Q. et al. Decoherence processes during optical manipulation of excitonic qubits in semiconductor quantum dots. *Phys. Rev. B* **72**, 035306 (2005).
30. Van Hattem, B. et al. From the artificial atom to the Kondo-Anderson model: orientation-dependent magnetophotoluminescence of charged excitons in InAs quantum dots. *Phys. Rev. B* **87**, 205308 (2013).
31. Rai, A. K. et al. Spatially indirect transitions in electric field tunable quantum dot diodes. *Phys. Status Solidi B* **253**, 437–441 (2016).
32. Carmele, A. et al. Formation dynamics of an entangled photon pair: a temperature-dependent analysis. *Phys. Rev. B* **81**, 195319 (2010).
33. Toda, Y., Moriwaki, O., Nishioka, M. & Arakawa, Y. Efficient carrier relaxation mechanism in InGaAs/GaAs self-assembled quantum dots based on the existence of continuum states. *Phys. Rev. Lett.* **82**, 4114–4117 (1999).
34. Vasanelli, A., Ferreira, R. & Bastard, G. Continuous absorption background and decoherence in quantum dots. *Phys. Rev. Lett.* **89**, 216804 (2002).
35. Schulhauser, C. et al. Emission from neutral and charged excitons in a single quantum dot in a magnetic field. *Physica E* **21**, 184–188 (2004).
36. Weiss, K. M., Miguel-Sanchez, J. & Elzerman, J. M. Magnetically tunable singlet-triplet spin qubit in a four-electron InGaAs coupled quantum dot. *Sci. Rep.* **3**, 3121 (2013).
37. Winger, M. et al. Explanation of photon correlations in the far-off-resonance optical emission from a quantum-dot–cavity system. *Phys. Rev. Lett.* **103**, 207403 (2009).
38. Ates, S. et al. Non-resonant dot–cavity coupling and its potential for resonant single-quantum-dot spectroscopy. *Nat. Photonics* **3**, 724 (2009).
39. Kaniber, M. et al. Investigation of the nonresonant dot-cavity coupling in two-dimensional photonic crystal nanocavities. *Phys. Rev. B* **77**, 161303 (2008).
40. Settnes, M., Kaer, P., Moelbjerg, A. & Mork, J. Auger processes mediating the nonresonant optical emission from a semiconductor quantum dot embedded inside an optical cavity. *Phys. Rev. Lett.* **111**, 067403 (2013).
41. Villas-Bôas, J. M., Ulloa, S. E. & Govorov, A. O. Decoherence of Rabi oscillations in a single quantum dot. *Phys. Rev. Lett.* **94**, 057404 (2005).
42. Villas-Bôas, J., Ulloa, S. E. & Govorov, A. O. Damping of coherent oscillations in a quantum dot photodiode. *Physica E* **26**, 337–341 (2005).
43. Urbaszek, B. et al. Temperature-dependent linewidth of charged excitons in semiconductor quantum dots: strongly broadened ground state transitions due to acoustic phonon scattering. *Phys. Rev. B* **69**, 035304 (2004).
44. Nicoll, C. et al. MBE growth of In (Ga) As quantum dots for entangled light emission. *J. Cryst. Growth* **311**, 1811–1814 (2009).
45. Ulrich, S. M. et al. Spectroscopy of the D_1 transition of cesium by dressed-state resonance fluorescence from a single (In,Ga)As/GaAs quantum dot. *Phys. Rev. B* **90**, 125310 (2014).

46. Portalupi, S. L. et al. Simultaneous faraday filtering of the mollow triplet sidebands with the Cs-D_1 clock transition. *Nat. Commun.* **7**, 13632 (2016).
47. Arzberger, M., Käsberger, U., Böhm, G. & Abstreiter, G. Influence of a thin AlAs cap layer on optical properties of self-assembled InAs/GaAs quantum dots. *Appl. Phys. Lett.* **75**, 3968 (1999).
48. Tsatsul'nikov, A. F. et al. Volmer–Weber and Stranski–Krastanov InAs-(Al, Ga)As quantum dots emitting at 1.3 μm. *J. Appl. Phys.* **88**, 6272 (2000).
49. Lu, X. M., Matsubara, S., Nakagawa, Y., Kitada, T. & Isu, T. Suppression of photoluminescence from wetting layer of InAs quantum dots grown on (311)b GaAs with AlAs cap. *J. Cryst. Growth* **425**, 106–109 (2015).
50. Tutu, F. et al. InAs/GaAs quantum dot solar cell with an AlAs cap layer. *Appl. Phys. Lett.* **102**, 163907 (2013).
51. Kuhlmann, A. V. et al. Charge noise and spin noise in a semiconductor quantum device. *Nat. Phys.* **9**, 570–575 (2013).
52. Leonard, D., Pond, K. & Petroff, P. M. Critical layer thickness for self-assembled InAs islands on GaAs. *Phys. Rev. B* **50**, 11687–11692 (1994).
53. Wasilewski, Z., Fafard, S. & McCaffrey, J. Size and shape engineering of vertically stacked self-assembled quantum dots. *J. Cryst. Growth* **201/202**, 1131–1135 (1999).
54. Vullum, P. E. et al. Quantitative strain analysis of InAs/GaAs quantum dot materials. *Sci. Rep.* **7**, 45376 (2017).
55. Blokland, J. et al. Ellipsoidal InAs quantum dots observed by cross-sectional scanning tunneling microscopy. *Appl. Phys. Lett.* **94**, 023107 (2009).
56. Smith, J. M. et al. Voltage control of the spin dynamics of an exciton in a semiconductor quantum dot. *Phys. Rev. Lett.* **94**, 197402 (2005).
57. Dreiser, J. et al. Optical investigations of quantum dot spin dynamics as a function of external electric and magnetic fields. *Phys. Rev. B* **77**, 075317 (2008).
58. Müller, K. et al. Probing ultrafast carrier tunneling dynamics in individual quantum dots and molecules. *Ann. Phys.* **525**, 49–58 (2013).
59. Warburton, R. J. et al. Optical emission from a charge-tunable quantum ring. *Nature* **405**, 926–929 (2000).
60. Urbaszek, B. et al. Fine structure of highly charged excitons in semiconductor quantum dots. *Phys. Rev. Lett.* **90**, 247403 (2003).
61. Ware, M. E. et al. Polarized fine structure in the photoluminescence excitation spectrum of a negatively charged quantum dot. *Phys. Rev. Lett.* **95**, 177403 (2005).
62. Kleemans, N. A. J. M. et al. Many-body exciton states in self-assembled quantum dots coupled to a Fermi sea. *Nat. Phys.* **6**, 534–538 (2010).
63. Warburton, R. J., Nicholas, R. J., Howard, L. K. & Emeny, M. T. Intraband and interband magneto-optics of p-type $In_{0.18}Ga_{0.82}As$/GaAs quantum wells. *Phys. Rev. B* **43**, 14124–14133 (1991).
64. Di Carlo, A. Microscopic theory of nanostructured semiconductor devices: beyond the envelope-function approximation. *Semicond. Sci. Technol.* **18**, R1 (2002).
65. Miller, B. T. et al. Few-electron ground states of charge-tunable self-assembled quantum dots. *Phys. Rev. B* **56**, 6764–6769 (1997).
66. Kouwenhoven, L. P., Austing, D. G. & Tarucha, S. Few-electron quantum dots. *Rep. Prog. Phys.* **64**, 701–736 (2001).
67. Bayer, M. et al. Fine structure of neutral and charged excitons in self-assembled In(Ga)As/(Al)GaAs quantum dots. *Phys. Rev. B* **65**, 195315 (2002).
68. Franceschetti, A., Wang, L. W., Fu, H. & Zunger, A. Short-range versus long-range electron-hole exchange interactions in semiconductor quantum dots. *Phys. Rev. B* **58**, R13367–R13370 (1998).
69. Rudin, S., Reinecke, T. L. & Bayer, M. Temperature dependence of optical linewidth in single InAs quantum dots. *Phys. Rev. B* **74**, 161305 (2006).
70. Kuhlmann, A. V. et al. Transform-limited single photons from a single quantum dot. *Nat. Commun.* **6**, 8204 (2014).

Acknowledgements

M.C.L., I.S., and R.J.W. acknowledge financial support from SNF Project No. 200020_156637 and from NCCR QSIT. This project received funding from the European Union Horizon 2020 Research and Innovation Program under the Marie Skłodowska-Curie grant agreement No. 747866 (EPPIC). S.S., J.R., A.L., and A.D.W. gratefully acknowledge financial support from the grants DFH/UFA CDFA05-06, DFG TRR160, DFG project 383065199, LU2051/1-1, and BMBF Q.Link.X 16KIS0867.

Author contributions

S.S. and A.L. initiated the project. S.S., J.R., and A.L. carried out the QD-growth and ensemble-PL-measurements together with A.D.W. T.D., A.K., and B.E.K. carried out the STEM and EDX analysis. M.C.L. and I.S. carried out the single-QD-spectroscopy. M.C.L., I.S., A.L., and R.J.W. developed concepts and established the links between the various aspects of the project. M.C.L. and R.J.W. wrote the paper with input from all authors.

Additional information

Supplementary information accompanies this paper at https://doi.org/10.1038/s42005-019-0194-9.

Competing interests: The authors declare no competing interests.

Reprints and permission information is available online at http://npg.nature.com/reprintsandpermissions/

Publisher's note: Springer Nature remains neutral with regard to jurisdictional claims in published maps and institutional affiliations.